JOURNAL OF GEOPHYSICAL RESEARCH, VOL. 106, NO. A1, PAGES 117–125, JANUARY 1, 2001

Ionospheric electrical conductances produced by auroral proton precipitation

Marina Galand[1]
Space Environment Center, National Oceanic and Atmospheric Administration, Boulder, Colorado

Arthur D. Richmond
High Altitude Observatory, National Center for Atmospheric Research, Boulder, Colorado

Abstract. From incoherent scatter radar observations and space-borne particle detector data, it appears that energetic proton precipitation can sometimes, for some locations, be a major source of ionization in the auroral ionosphere and contribute significantly to the electrical conductances. Here we propose a simple parameterization for the Pedersen and Hall conductances produced by proton precipitation. The derivation is based on a proton transport code for computing the electron production rate and on an effective recombination coefficient for deducing the electron density. The atmospheric neutral densities and temperatures and the geomagnetic-field strength are obtained from standard models. The incident protons are assumed to have a Maxwellian distribution in energy with a mean energy $\langle E \rangle$ in the 2-40 keV range and an energy flux Q_0. The parameterized Pedersen and Hall conductances are functions of $\langle E \rangle$ and Q_0, as well as of the geomagnetic-field strength. The dependence on these quantities is compared with those obtained for electron precipitation and for solar EUV radiation. To add the contribution of proton precipitation to the total conductances for electrodynamic studies in auroral regions, the conductances produced by electron and proton precipitations can be combined by applying a root-sum-square approximation.

1. Introduction

The concept of ionospheric conductances, or height-integrated conductivities, is useful in studies of the electrodynamics of the high-latitude ionosphere. Because large parallel electrical conductivity along the nearly vertical geomagnetic field prevents the establishment of any significant vertical electric potential gradients, the horizontal electric field is nearly constant in altitude. Therefore the height-integrated horizontal current density associated with the electric field can be directly computed from the conductances. It is crucial to have an accurate conductance model in order to infer Birkeland currents and electric field patterns from magnetometer data [*Doyle et al.*, 1986; *Rich et al.*, 1987, 1991] or to estimate the Joule heating from particle and electric field measurements [*Richmond and Kamide*, 1988]. Nevertheless, to date, in the electrical conductance models applied to the high-latitude regions, energetic electrons have been the only particles of magnetospheric origin taken into account as a source of ionization [*Wallis and Budzinski*, 1981; *Reiff*, 1984; *Fuller-Rowell and Evans*, 1987; *Hardy et al.*, 1987; *Brekke and Moen*, 1993]. Energetic protons have been either neglected or treated as if they were electrons, which is not an appropriate way to infer their electron production rate, as explained by *Galand et al.* [1999].

Even though energetic protons are not a dominant energy source in the high-latitude region overall, their contribution to the total auroral energy flux represents on the average about 15% that of electrons [*Hardy et al.*, 1989], and they can be important at given locations and times, particularly in the cusp and at the equatorward boundary of the auroral oval before midnight, as particle observations from polar-orbiting satellites [*Hardy et al.*, 1989, 1991; *Newell et al.*, 1991] and ground-based optical H emission observations [*Creutzberg et al.*, 1988] attest. Emphasizing these results, *Robinson and Vondrak* [1985], relying on incoherent scatter radar measurements, and *Basu et al.* [1987], *Senior et al.* [1987], and *Lilensten and Galand* [1998], using simultaneous space- and ground-based observations from a satellite and an incoherent scatter radar, have shown that protons are sometimes the major source of ionization and can therefore contribute significantly to enhance the

[1]Now at Center for Space Physics, Boston University, Boston, Mass.

Copyright 2001 by the American Geophysical Union.

Paper number 1999JA002001.
0148-0227/01/1999JA002001$09.00

conductivities [*Anderson et al.*, 1997; *Galand et al.*, 1999]. Finally, *Senior* [1991] studied the particle precipitation contribution to the height-integrated conductivities. She compared her results derived from European Incoherent SCATter radar (EISCAT) data with a statistical model of conductances obtained from precipitating electron characteristics measured by the polar-orbiting DMSP satellites [*Hardy et al.*, 1987]. She found that the EISCAT-derived conductances agree well with the DMSP model in the morning sector but are systematically larger than the model in the evening sector. She suggested that this difference is due to E region electron production by energetic ion precipitation, which occurs preferentially in the evening sector.

For these cases where protons are a significant, and sometimes major, ionization source, we propose here, for the first time, a simple way to parameterize the Pedersen and Hall conductances. We first present in detail the calculation of the perpendicular electrical conductances produced by proton precipitation, assuming a Maxwellian distribution in energy and a mean energy in the 2-40 keV range. We next discuss the dependence of these conductances on the mean energy of the incident protons and compare our results with the conductances associated with electron precipitation. We then study the dependence of proton-produced conductances on the geomagnetic-field strength and compare with that obtained for solar EUV radiation. Finally, we propose a parameterization for the Pedersen and Hall conductances produced by proton precipitation, and we discuss how conductances inferred from different sources of ionization can be combined.

2. Pedersen and Hall Conductances Produced by Energetic Protons

To calculate the perpendicular electrical conductances produced by proton precipitation, three steps are performed: first, we compute the electron production as a function of altitude associated with the interaction of a proton beam with the atmosphere; second, we derive the electron density profile; and third, we determine the Pedersen and Hall conductivities and integrate them in altitude.

For the computation of the electron production rate P_e associated with an incident proton beam, we use the transport code developed by *Galand* [1996], which solves the steady-state Boltzmann equations for protons and H atoms. The particle fluxes are computed as a function of altitude, energy, and pitch angle, starting from a specified incident flux at the top of the atmosphere. The solution is based on the introduction of dissipative forces to describe the energy loss through collisions [*Galand et al.*, 1997]. This proton transport code has been successfully validated by comparison with rocket particle data [*Søraas et al.*, 1974] and by comparison with the model of *Basu et al.* [1993] [*Galand et al.*, 1997]. From the computed particle fluxes and from the neutral densities and the ionization and stripping cross sections, it is possible to determine the ionization rate produced directly by the proton beam. From this primary electron production P_{e1}, a secondary electron production P_{e2} can be estimated as proposed by *Lilensten and Galand* [1998]: $P_{e2} = P_{e1} \times 0.006\, E_0$, where P_{e1} and P_{e2} are in $m^{-3}\ s^{-1}$ and the Maxwellian characteristic energy E_0 in keV is in the 1-50 range. This additional ionization is created by the proto-electrons, energetic electrons directly produced by the interaction of the proton beam with the atmosphere, that is, the electrons generated through the primary production. Note that this secondary electron production is less than 12% of the primary production when $E_0 < 20$ keV. The total electron production P_e is the sum of P_{e1} and P_{e2}.

The incident flux at the top of the atmosphere is assumed to be purely protons and isotropic over the downward hemisphere. Observations from sounding rockets and from satellites support this pitch angle distribution [e.g., *Søraas et al.*, 1974; *Urban*, 1981]. However, observations indicate that sometimes the pitch-angle distribution is anistropic, peaking along the magnetic-field lines [*Urban*, 1981]. We have tested such a distribution, but the change in the conductances is only a few percent increase. Moreover, the incident proton flux is assumed to have a Maxwellian distribution in energy. The mean energy of the Maxwellian, $\langle E \rangle$, is varied from 2 to 40 keV, typical for auroral proton precipitation [*Hardy et al.*, 1989]. For a Maxwellian distribution, the characteristic energy E_0 is half of the mean energy $\langle E \rangle$; that is, E_0 varies from 1 to 20 keV. The total incident energy flux integrated over pitch angle and energy, Q_0, is chosen as 1 mW m^{-2}, providing normalized results. The neutral atmosphere is specified by the Mass Spectrometer and Incoherent Scatter model (MSIS-90) [*Hedin*, 1991], for the location of Chatanika (65.1°N, −147.4°E) at 2200 local time (LT) in winter, with a magnetic activity index A_p of 20 and a solar index $F_{10.7}$ of 150, representative of average magnetic and solar conditions. The exospheric temperature is 970 K. The collision cross section set used is from *Basu et al.* [1987] and from *Rees* [1989]. The collisional energy losses are those presented by *Galand et al.* [1997]. The incident beam is assumed sufficiently broad (larger than 250 km) that beam spreading associated with the horizontal diffusion of the hydrogen atoms can be neglected [*Jasperse and Basu*, 1982]. No field-aligned electric field or collisional angular redistribution is considered. The mirroring effect of the magnetic field is not included, as it does not have a significant effect on the electron production rate [*Galand and Richmond*, 1999]. The dip angle is 90°. As for numerical inputs, the altitude grid extends from 800 km down to 90 km on 200 levels. The minimum energy of the energy grid is 100 eV, and the maximum energy is at least $10 \times \langle E \rangle$. The number of levels for the energy grid is between 100 and 150. The pitch angle cosine grid is uniform with 10 levels. Figure 1a shows the altitude profiles of the electron production rate ob-

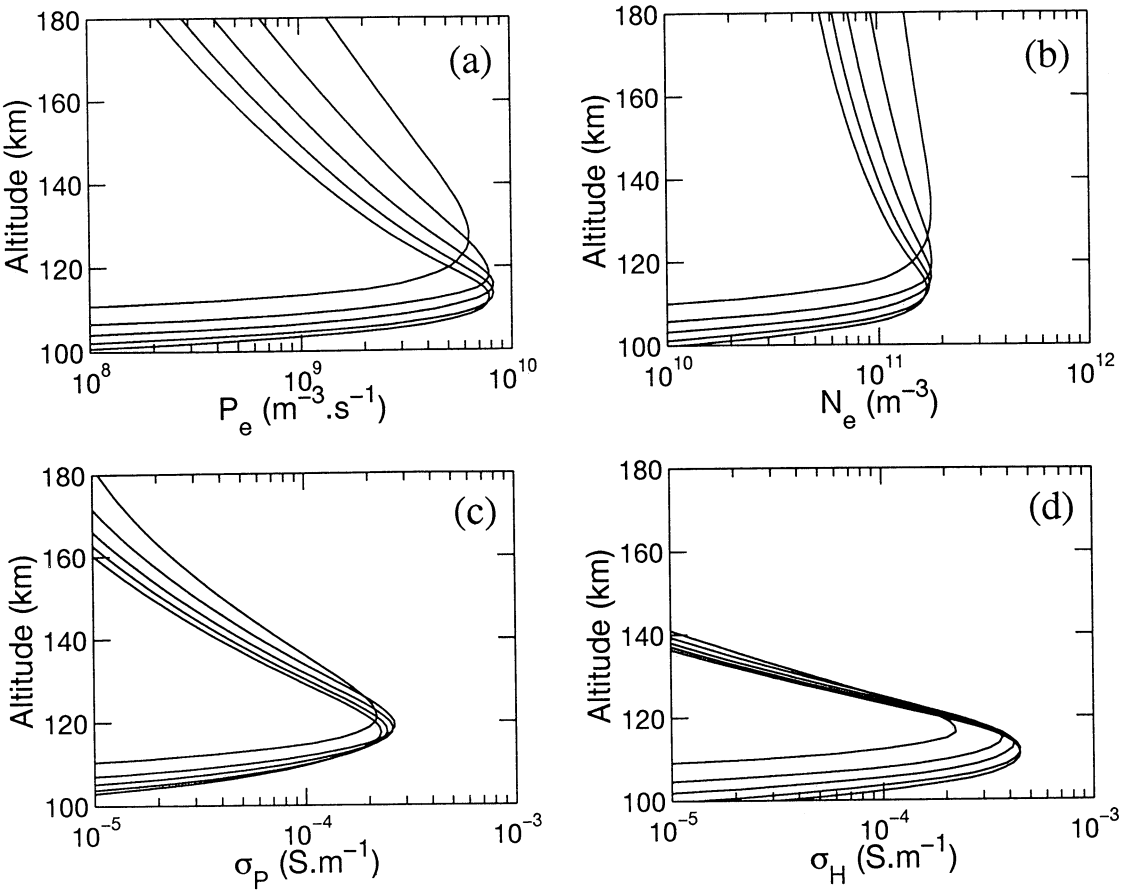

Figure 1. Results for incident proton fluxes with a Maxwellian distribution in energy and a normalized energy flux of 1 mW m^{-2}, for the location of Chatanika. The mean energies $\langle E \rangle$ are 2, 10, 20, 30, and 40 keV, lines from top to bottom, respectively. (a) Altitude profiles of the electron production rate P_e. (b) Altitude profiles of the electron density N_e. (c) Altitude profiles of the Pedersen conductivity σ_P. (d) Altitude profiles of the Hall conductivity σ_H.

tained for five different mean energies $\langle E \rangle$ chosen between 2 and 40 keV. As expected, the higher the mean energy $\langle E \rangle$, the deeper the energetic particles penetrate into the atmosphere, and the lower the altitude of the peak lies. Note that the spread in altitude of the peaks is relatively small, lying between 110 and 125 km.

The second step consists in deducing the electron density N_e from the electron production rate as a function of altitude z. In the E region the electrons are essentially in photochemical equilibrium, and loss is through dissociative recombination with molecular ions, whose density is nearly the same as the electron density, so that we can use the approximation

$$N_e(z) = \sqrt{\frac{P_e(z)}{\alpha_{\text{eff}}(z)}}, \qquad (1)$$

where α_{eff} is the effective mean recombination coefficient. This coefficient depends on ion composition and electron temperature, parameters that are variable and not well known for any given time and location. An empirically estimated average recombination coefficient [*Wickwar et al.*, 1975; *Oran et al.*, 1981; *Vickrey et al.*, 1982] for the altitude range 90-180 km is

$$\alpha_{\text{eff}}(z) = 2.50 \times 10^{-12} \exp\left(\frac{-z}{51.2}\right), \qquad (2)$$

where α_{eff} is in m^3 s^{-1} and z is in kilometers. From (1) and (2) the electron density profile can be computed up to 180 km. That is the top altitude for our conductivity calculations, since the contribution to the height-integrated conductivities from higher altitudes is negligible. This also avoids the problem of departures from chemical equilibrium as diffusive transport becomes important at high altitudes. The height profiles of N_e, presented in Figure 1b, are less spread in relative magnitude as compared with the profiles of P_e. Note that the use of a transport code along with the relation (1) to compute the electron density profile has been validated by the analysis of combined experiments between a satellite measuring the incident particle flux and an incoherent scatter radar observing the electron density profile [*Basu et al.*, 1987; *Senior et al.*, 1987; *Lilensten and Galand*, 1998].

In the third step, we determine the Pedersen and Hall conductivities, noted σ_P and σ_H, respectively. For current $\mathbf{J}_\perp$ perpendicular to the geomagnetic field $\mathbf{B}$, the Pedersen conductivity gives the component in the direction of the electric field $\mathbf{E}_\perp$, while the Hall conductivity gives the component in the direction perpendicular to both $\mathbf{E}$ and $\mathbf{B}$:

$$\mathbf{J}_\perp = \sigma_P \mathbf{E}_\perp + \sigma_H \frac{\mathbf{B}}{B} \times \mathbf{E}. \quad (3)$$

The current density is the sum over the various charged species of their charge density multiplied by their velocity. To a good approximation, the velocity can be obtained by balancing the Lorentz force and the frictional force caused by collisions with neutrals [e.g., *Richmond*, 1995]. The resultant conductivity expressions are

$$\sigma_P = \sum_{i=O_2^+,NO^+,O^+} \sum_{n=N_2,O_2,O} \frac{N_i\, e}{B} \left(\frac{\nu_{en\perp}\, \Omega_e}{\nu_{en\perp}^2 + \Omega_e^2} + \frac{\nu_{in}\, \Omega_i}{\nu_{in}^2 + \Omega_i^2} \right) \quad (4)$$

$$\sigma_H = \sum_{i=O_2^+,NO^+,O^+} \sum_{n=N_2,O_2,O} \frac{N_i\, e}{B} \left(\frac{\Omega_e^2}{\nu_{en\perp}^2 + \Omega_e^2} - \frac{\Omega_i^2}{\nu_{in}^2 + \Omega_i^2} \right), \quad (5)$$

where σ_P and σ_H are in S m^{-1}, N_i is the density of the ion species i in m^{-3}, e is the magnitude of the electron charge in coulomb, and B is the magnitude of the geomagnetic field in tesla. Here Ω_e and Ω_i are the angular gyrofrequencies in s^{-1} of the electrons and the ion species i, respectively: $\Omega = eB/m$, where m is the mass of the particle (electron or ion) in kilograms. Here $\nu_{en\perp}$ represents the effective collision frequency between the electrons and the neutral species n for motions perpendicular to $\mathbf{B}$, and ν_{in} is the (isotropic) collision frequency between the ion species i and the neutral species n. We compute B from the International Geomagnetic Reference Field model (IGRF-90) [*Langel*, 1992] for epoch 1994. For the collision frequencies, we use the formulas from *Richmond* [1995, Table 9.2.1], except that the term $8.9 \times 10^{-16}\, N_O\, (T_r/500)^{0.5}$ representing ν_{O^+-O} in m^3 s^{-1} has been replaced by $3.0 \times 10^{-17}\, N_O\, \sqrt{T_r}\, [1. - 0.135 \log_{10}(T_r/1000)]^2$ [*Pesnell*, 1993], where T_r in K is the average of the O and the O^+ temperatures and N_O in m^{-3} is the number density of O. For the computation of the collision frequencies, the electron and ion temperatures are obtained from the International Reference Ionosphere (IRI-90) [*Bilitza*, 1990] for a 12-month running mean of solar sunspot number equal to 102, on December 5, 1994, at Chatanika, and the neutral densities and temperature are from the MSIS-90 model [*Hedin*, 1991]. The ion densities are deduced from the computed electron density, taking the relative ion composition from the IRI model. The altitude profiles of the Pedersen and Hall conductivities are shown for different values of $\langle E \rangle$ in Figures 1c and 1d, respectively. The Pedersen conductivities peak around 120 km with a magnitude of $\sim 2.5 \times 10^{-4}$ S m^{-1}, whereas the Hall conductivities peak below, between 110 and 120 km, with peak magnitudes between 2 and 5 $\times 10^{-4}$ S m^{-1}. The Pedersen conductivities are significant over a broader range of altitudes than are the Hall conductivities, which are largely confined between 100 and 140 km.

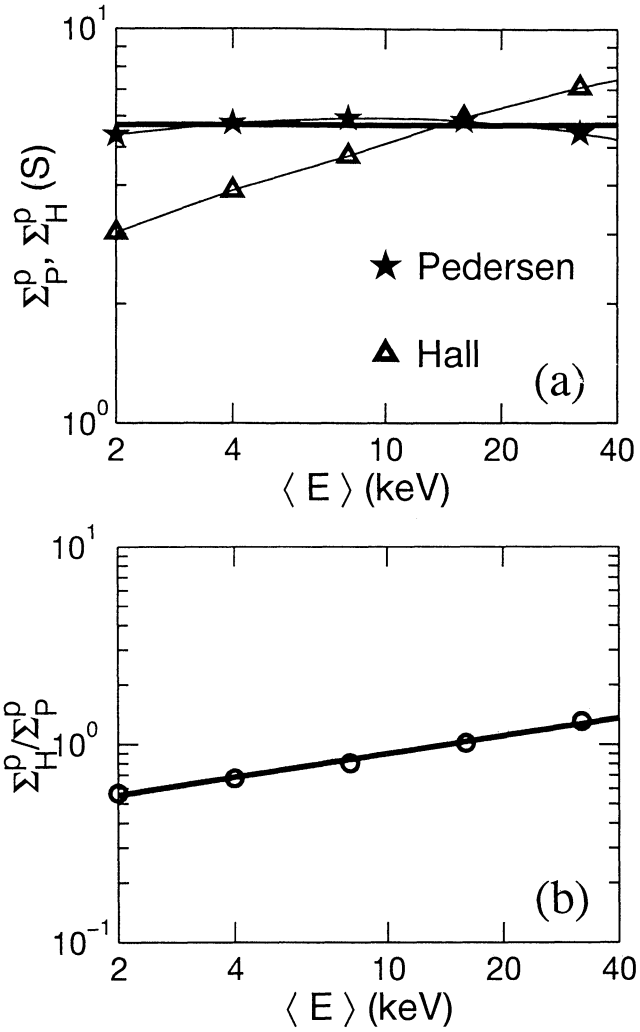

Figure 2. Results for incident proton fluxes with a Maxwellian distribution in energy and a normalized energy flux of 1 mW m^{-2}, for the location of Chatanika. Note that the mean energy $\langle E \rangle$ is equal to twice the characteristic energy E_0 of the incident protons. (a) The conductances deduced from equations (4) and (5) using the proton transport code for the electron production are plotted with thin solid lines as a function of the mean energy $\langle E \rangle$ of the incident protons. The Pedersen conductance Σ_P^p is presented with stars and the Hall conductance Σ_H^p with triangles. The thick solid line is from the parameterization (6). (b) The conductance ratio Σ_H^p/Σ_P^p is plotted as a function of the characteristic energy $\langle E \rangle$ of the incident protons. The ratio obtained from the proton transport code is shown by the circles. The fitted ratio represented by (7) is plotted as a thick solid line.

The Pedersen conductance Σ_P^p and the Hall conductance Σ_H^p, that is, the height integrals of the respective conductivities, are shown in thin solid lines with stars and with triangles, respectively, in Figure 2a. They are plotted as functions of the mean energy $\langle E \rangle$ of the incident protons. Since the peak Pedersen conductivity and the shape of its altitude profile are relatively insensitive to the mean energy $\langle E \rangle$ of the incident protons (Figure 1c), the Pedersen conductance does not vary significantly with $\langle E \rangle$ and can be considered as approximately constant in the 2-40 keV range of $\langle E \rangle$. However, the Hall conductance is more sensitive to a variation in $\langle E \rangle$ (Figure 1d), and the ratio of Hall to Pedersen conductance varies with $\langle E \rangle$, as shown in Figure 2b. Because softer protons produce ionization at higher altitudes, the Pedersen conductance is larger than the Hall conductance for low $\langle E \rangle$. As $\langle E \rangle$ increases, protons penetrate more deeply into the atmosphere and result in a larger Hall conductance. Therefore the ratio of Hall to Pedersen conductance increases with the mean energy $\langle E \rangle$.

We tested the sensitivity of the conductances to the assumed atmospheric model, by carrying out additional runs for different times of day and seasons and with different relative ion compositions (as they enter into the collision frequency calculation), and found differences of at most 3%, which are negligible in comparison with uncertainties and variability of the effective recombination coefficient. We did not test the effects of atmospheric variability with solar cycle but expect them also to be relatively small. We tested the parameterization by *Galand et al.* [1999] for the primary electron production in our conductance calculations (see Galand et al.'s (1), (2), (10), and (11) and their Tables 1 and 2). The parameterized electron production is calculated between 90 and 800 km, on the basis of the mean energy $\langle E \rangle$ and the energy flux Q_0 of the incident protons as well as the height profiles of the neutral densities. The relative differences between the conductances using the parameterized production and those computed directly from the proton transport is less than 6% for the Pedersen conductance and less than 5% for the Hall conductance. These values are compatible with the 10% parameterization error for the peak production rate.

3. Dependence of Conductances on the Mean Energy $\langle E \rangle$

3.1. Parameterization for Proton Precipitation at Chatanika

We propose to parameterize the Pedersen and Hall conductances as a function of the mean energy $\langle E \rangle$ from the results obtained in section 2. Because the Pedersen and Hall conductances are proportional to the electron density, that is, approximately to the square root of the electron production rate (see (1)), we expect them to vary approximately as the square root of the incident energy flux Q_0. Inspection of Figure 2a suggests the following parameterization for conductances produced purely by proton precipitation:

$$\Sigma_P^p = 5.7\ Q_0^{0.5} \tag{6}$$

$$\frac{\Sigma_H^p}{\Sigma_P^p} = 0.45\ \langle E \rangle^{0.3}, \tag{7}$$

where Σ_P^p and Σ_H^p are in Siemens, Q_0 is in mW m^{-2}, and $\langle E \rangle$ is in keV, between 2 and 40. The simplified relations (6) and (7) are plotted with thick solid lines in Figures 2a and 2b, respectively. The fitted values are within 9% and 6% of the actual values for the Pedersen conductance and for the Hall to Pedersen conductance ratio, respectively.

3.2. Comparison With Electron Precipitation

Relations analogous to (6) and (7) have been derived for auroral electron precipitation. The formulas proposed by *Robinson et al.* [1987] have been widely used, for example, for deriving global patterns of conductances [*Hardy et al.*, 1987], as input of the Assimilative Mapping of Ionospheric Electrodynamics (AMIE) procedure [*Richmond and Kamide*, 1988], in determining the electric field from magnetic field and particle flux observations [*Rich et al.*, 1987, 1991], in studying the longitudinal variations of electrodynamical quantities [*Gasda and Richmond*, 1998], and in estimating the energy flux and mean energy of precipitating electrons from auroral conductances [*Ahn et al.*, 1998]. The parameterized Pedersen and Hall conductances Σ_P^e and Σ_H^e proposed by Robinson et al. for electron precipitation are functions of the mean energy $\langle E \rangle$ and energy flux Q_0 of the incident electrons:

$$\Sigma_P^e = \frac{40\ \langle E \rangle}{16 + \langle E \rangle^2}\ Q_0^{0.5} \tag{8}$$

$$\frac{\Sigma_H^e}{\Sigma_P^e} = 0.45\ \langle E \rangle^{0.85}, \tag{9}$$

where Σ_P^e and Σ_H^e are in S, Q_0 is in mW m^{-2}, and $\langle E \rangle$ is in keV, between 0.5 and 20. This parameterization is derived from the work of *Vickrey et al.* [1981], using an energy deposition function to compute the ionization rate [*Rees*, 1963; *Berger et al.*, 1970] and adopting the same effective recombination coefficient (2) that we use. The incident electron flux is assumed to be isotropic with a Maxwellian distribution in energy. By calculating conductances produced by several other types of distributions, *Robinson et al.* [1987] showed that the relations (8) and (9) are valid for most common auroral electron spectra. The conductivities were computed by standard methods, using a standard model for the thermospheric state [*Banks and Kockarts*, 1973]. *Watermann et al.* [1993] found reasonably good agreement between conductances estimated with formulas (8) and (9), using electron flux data from the DMSP-F7 satellite, and conductances calculated using electron density observations from the Sondrestrom incoherent scatter radar in early morning. *Germany et al.* [1994] and

Rees et al. [1995] calculated model conductances that agree reasonably well with formulas (8) and (9). *Germany et al.* [1994] also discussed the validity of using an effective recombination coefficient, comparing it against a full ion chemistry model. The latter predicts dependencies of the conductances on Q_0 with powers somewhat greater than 0.5, depending on the particle mean energy, owing to the fact that the dependence of the electron loss rate on electron density becomes less quadratic and more linear at higher altitudes, above 150 km.

Comparing (6) and (8), we see that whereas Σ_P^p is essentially independent of the mean energy of the incident protons in the range 2-40 keV, Σ_P^e depends significantly on the mean energy of the incident electrons. The difference can be attributed to the different manner in which the energy loss function varies with energy for protons and for electrons. Above 200 eV, the energy loss function increases with energy for protons [*Kozelov and Ivanov*, 1992; *Galand*, 1996] but decreases with increasing energy for electrons [*Jones*, 1974]. Consequently, as the initial energy of a proton is increased it loses energy more rapidly and achieves only a modest amount of additional penetration into the atmosphere; however, as the energy of an electron is increased, it loses energy more slowly and penetrates much more deeply into the atmosphere. Therefore the ionization rate of protons peaks in a smaller range of altitudes compared with electrons [*Strickland et al.*, 1993]. Since the ion Pedersen mobility maximizes around 120 km, ionization near that altitude contributes most effectively to the Pedersen conductance. The altitude of peak ionization by protons of 2-40 keV mean energy never differs by more than 8 km from 120 km (Figure 1a). By contrast, ionization by electrons of 1 keV mean energy peaks much higher, while ionization by electrons with 20 keV mean energy peaks much lower than 120 km, accounting for the falloff in Σ_P^e for these low and high mean energies.

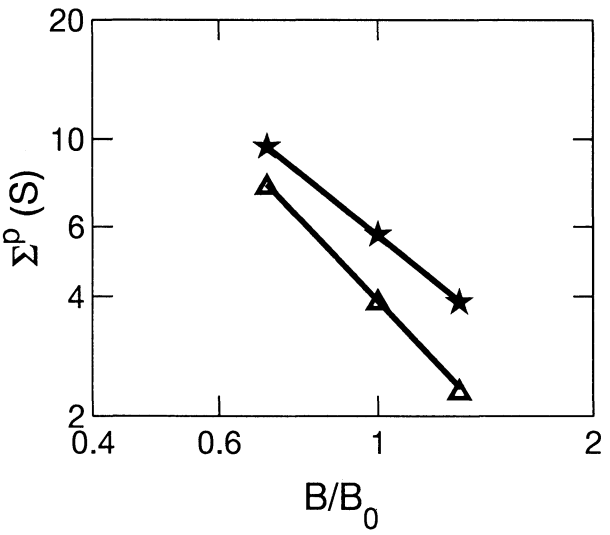

Figure 3. Perpendicular conductances for an incident proton flux with a Maxwellian distribution in energy, with a mean energy $\langle E \rangle$ of 4 keV and a normalized energy flux of 1 mW m^{-2}. The conductances deduced from equations (4) and (5) are shown with stars (Σ_P^p) and with triangles (Σ_H^p). The thick solid lines are from the parameterizations (10) and (11). The conductances are presented as a function of the geomagnetic-field strength B at 110 km normalized to the value $B_0 = 54$ μT, valid over Chatanika.

From (8), we can deduce that Σ_P^e reaches its maximum at $\langle E \rangle = 4$ keV with a value of 5 S for $Q_0 = 1$ mW m^{-2}. At $\langle E \rangle = 20$ keV, its value is reduced to 1.9 S. However, Σ_P^p from (6) is constant with a value of 5.7 S. The higher values obtained for Σ_P^p compared with Σ_P^e are due both to the effect discussed above concerning the altitudes of ionization by electrons and to different values of energy loss per ion-electron pair produced, lower for protons than for electrons [*Strickland et al.*, 1993; *Galand et al.*, 1999]. For given values for $\langle E \rangle$ and Q_0, protons produce more total ionization than do electrons.

Similarly to the Pedersen conductance, the dependence of the Hall to Pedersen conductance ratio on $\langle E \rangle$ is greater for electrons than for protons. However, in both cases it increases with $\langle E \rangle$, since the Hall conductivity lies at low altitudes where the electron production increases most strongly with increasing $\langle E \rangle$.

4. Dependence of Conductances on the Geomagnetic-Field Strength

4.1. Parameterization for Proton Precipitation at $\langle E \rangle = 4$ keV

Wallis and Budzinski [1981] pointed out that geographical variations in the geomagnetic-field strength can significantly affect the conductances. The calculations we discussed in section 2 are valid for the location of Chatanika, where the magnetic-field strength is close to that of the Earth's dipole (see *Gasda and Richmond*, 1998, Figure 3, for magnetic longitude −95°). At an altitude of 110 km that field strength is 54 μT, which we shall use to define a reference value B_0. If we search all locations poleward of 60° north or south magnetic latitude, we find a minimum field strength at 110 km of 35 μT between Africa and Antarctica, at geographic coordinates −61.5°N, 30°E, and a maximum of 64 μT between Australia and Antarctica around −60°N, 140°E.

In order to investigate how variability of the geomagnetic-field strength affects the Pedersen and Hall conductances, we perform similar runs as in section 2, except for different B values within ± 30% of B_0. The dip angle is kept at 90°. The mean energy $\langle E \rangle$ is set at 4 keV and the energy flux Q_0 is set at 1 mW m^{-2}. The resultant conductances are shown in Figure 3. The straight lines correspond to the following parameterizations:

$$\Sigma_P^p = 5.7 \left(\frac{B}{B_0} \right)^{-1.45} \tag{10}$$

$$\Sigma_H^p = 3.9 \left(\frac{B}{B_0} \right)^{-1.90}, \tag{11}$$

where Σ_P^p and Σ_H^p are in S. Note that the value of 3.9 is deduced from $5.7 \times (0.45 \times 4^{0.3})$, obtained from relations (6) and (7). The fitted values are within 1 and 3% of the actual values for the Pedersen and Hall conductances, respectively.

As a test, we performed new simulations using the proton transport code applied to the location of the EISCAT incoherent scatter radar at Trømsø (96.5°N, 19.2°E), for which $(B/B_0) = 0.93$. The parameterized relations fit well the conductances obtained with the full model.

4.2. Comparison With Solar-EUV Conductances

Solar EUV and X-ray radiations are the major source of ionization of the dayside ionosphere. *Richmond* [1995] derived the following formulas for daytime values of the Pedersen and Hall conductances at mid latitudes for values of the solar zenith angle χ less than 80°:

$$\Sigma_P^{\mathrm{EUV}} = 11 \left(\frac{F_{10.7}}{100}\right)^{1.1} \left(\frac{B}{50\mu T}\right)^{-1.6} (\cos\chi)^{0.5} \quad (12)$$

$$\Sigma_H^{\mathrm{EUV}} = 14 \left(\frac{F_{10.7}}{100}\right)^{0.5} \left(\frac{B}{50\mu T}\right)^{-1.3} (\cos\chi)^{0.8} \quad (13)$$

where Σ_P^{EUV} and Σ_H^{EUV} are in S and where B represents the magnetic-field strength at 125 km. These relations were obtained using the MSIS-90 and IRI-90 models at 45°N, 2°E for different times of day, different seasons, and different levels of solar activity, and for arbitrary variations of the magnetic field strength at this location.

By comparing relations (10) with (12) and (11) with (13), we deduce that Σ_P^p is less strongly dependent on B than is Σ_P^{EUV}, whereas Σ_H^p is more strongly dependent on B than is Σ_H^{EUV}. In order to explain these results, let us consider how the conductivities depend on B at different altitudes, for given ion and electron densities and collision frequencies. At low altitudes, 100-110 km, $\nu_{en\perp} \ll \Omega_e$ and $\nu_{in} \gg \Omega_i$, and we can deduce from (4) and (5) that $\sigma_P \propto B^0$ and $\sigma_H \propto B^{-1}$. At high altitudes, above 140 km, $\nu_{en\perp} \ll \Omega_e$ and $\nu_{in} \ll \Omega_i$, and $\sigma_P \propto B^{-2}$ and $\sigma_H \propto B^{-3}$. We can therefore expect the power-law dependence on B to have a power between 0 and -2 for Σ_P and between -1 and -3 for Σ_H. Whether the power lies closer to the first or to the second limit depends on whether the bulk of the contribution to the height-integrated conductivity comes from below or above the transition altitude where $\nu_{in} = \Omega_i$, around 120 km. The vertical profiles of proton-produced electron density extend less strongly into the F region than do the profiles of solar-EUV-produced electron density, accounting for the weaker B-dependence of Σ_P^p than Σ_P^{EUV}. Likewise, the profiles of proton-produced electron density extend less deeply below the transition altitude than do the profiles of solar-EUV-produced electron density, accounting for the stronger B-dependence of Σ_H^p than Σ_H^{EUV}.

5. Discussion and Conclusions

The main purpose of this study has been to investigate the influence of proton precipitation on perpendicular electrical conductances. The calculation of the height-integrated conductivities is based on a proton transport code for computing the electron production rate and of an effective recombination coefficient for determining the electron density. The atmospheric temperatures, the neutral densities, and the geomagnetic field strength are obtained from standard models. Assuming a Maxwellian distribution in energy for the incident protons, we have studied the dependence of conductances on the mean energy $\langle E \rangle$ of the incident beam and on the geomagnetic-field strength B. From (6), (7), (10), and (11), we deduce the following parameterizations for the Pedersen and Hall conductances produced by an incident proton beam:

$$\Sigma_P^p = 5.7\ Q_0^{0.5} \left(\frac{B}{B_0}\right)^{-1.45} \quad (14)$$

$$\Sigma_H^p = 2.6\ \langle E \rangle^{0.3}\ Q_0^{0.5} \left(\frac{B}{B_0}\right)^{-1.90}, \quad (15)$$

where Σ_P^p and Σ_H^p are in S, Q_0 is the incident energy flux in mW m^{-2}, $\langle E \rangle$ is the mean energy in keV between 2 and 40, B is the geomagnetic-field strength at 110 km, and $B_0 = 54\mu$T. Note that 2.6 is 5.7×0.45, from (6) and (7).

When applying these relations to data from particle detectors limited to 20 keV or so, which are common for low-altitude polar-orbiting satellites, one should keep in mind the possible need to apply a correction factor to Q_0 to account for unmeasured energies above 20 keV. Concerning our assumption of a Maxwellian energy distribution for the protons, observations indicate that this is reasonable over the 1-30 keV energy range but does not take into account the high-energy tail that proton beams seem to have [*Decker et al.*, 1996, and references therein; *Codrescu et al.*, 1997]. However, we expect that the non-Maxwellian character of the proton distribution will have relatively less influence on the conductance parameterization than is the case for electron precipitation because of the fact that the vertical distribution of ionization is less dependent on particle energy for the proton case. *Robinson et al.* [1987] showed that the conductances produced by electrons are relatively insensitive to the shape of the energy spectrum. The conductances produced by protons should be even less sensitive to the shape of the energy spectrum.

The dependence on $\langle E \rangle$ of the conductances produced by proton precipitation is much weaker than that for electron precipitation. In addition, for a given value of Q_0, the Pedersen conductance produced by protons is greater. We can conclude that even though protons usually carry less energy flux than electrons at the top of the auroral ionosphere, the effect of protons on the Pedersen conductance and on the calculation of currents

and Joule heating can be significant. This is especially true for particular locations and times, like the equator edge of the auroral oval before midnight, where protons are often the major incident energy source.

We found that the conductances have a fairly strong inverse dependence on the geomagnetic-field strength B. The different relative contributions to the height-integrated conductivities above and below the altitude where $\nu_{in} = \Omega_i$ helps determine the strength of the B-dependence and explains the somewhat different B-dependencies for proton-produced and solar-EUV-produced conductances.

One of the main goals of this paper is to propose simple formulas for Pedersen and Hall conductances produced by proton precipitation, suitable for several purposes: for quick estimation of the contribution of protons in studies analogous to that by *Watermann et al.* [1993]; for deriving global patterns of conductances, from satellite particle data as by *Fuller-Rowell and Evans* [1987] and *Hardy et al.*, [1987] or from H emission observations which will be carried out on a global scale by the IMAGE satellite; or for including in global electrodynamic models [e.g., *Richmond et al.*, 1992], which have neglected, to date, the proton contribution to conductances. The dominant ionization sources included in global models are the solar-EUV radiation and, at high latitudes, the auroral electron precipitation. The background radiation, namely galactic EUV, cosmic radiation, and scattered EUV sunlight, and, at lower latitudes, the weak precipitation from the radiation belts represent minor ionization sources [*Wallis and Budzinski*, 1981]. With this whole variety of ionization sources, it is crucial to discuss how to combine two conductances, say, Σ_1 and Σ_2, arising from two different processes. On the one hand, if the sources were strictly separated in altitude, one could simply add the conductances. However, the altitudes usually overlap. On the other hand, if the source altitude distributions were identical, the ionization rates would add in the same proportion at every altitude, and the electron density at each altitude would scale by a constant factor as the square root of the summed production rates, yielding $\Sigma_{\text{total}} = \sqrt{\Sigma_1^2 + \Sigma_2^2}$. For combining solar-EUV-produced and particle-produced conductances, this estimate of the root-sum-square is far more accurate than a simple sum. *Wallis and Budzinski* [1981] estimated the error produced by the root-sum-square approximation to 7% for Σ_P and 15% for Σ_H. Such a method of combining conductances from solar-EUV radiation and auroral electron precipitation has been widely used in the literature [*Reiff*, 1984; *Rich et al.*, 1987, 1991; *Richmond and Kamide*, 1988; *Senior*, 1991; *Watermann et al.*, 1993]. Since typical ionization profiles by protons are not greatly different from those by electrons, it seems reasonable also to apply the root-sum-square approximation to combine conductances from electron and proton sources.

Acknowledgments. M.G. gratefully acknowledges the financial support of the National Research Council and the Space Environment Center. The work of A.D.R. was supported in part by NASA Award W-17,384. NCAR is sponsored by the National Science Foundation.

Janet G. Luhmann thanks Catherine Senior and Yukihiro Takahashi and another referee for their assistance in evaluating this paper.

References

Ahn, B.-H., A. D. Richmond, Y. Kamide, H. W. Kroehl, B. A. Emery, O. de la Beaujardière, and S.-I. Akasofu, An ionospheric conductance model based on ground magnetic disturbance data, *J. Geophys. Res.*, *103*, 14,769-14,780, 1998.

Anderson, P. C., I. W. McCrea, D. J. Strickland, J. B. Blake, and M. D. Looper, Coordinated EISCAT/DMSP measurements of electron density and energetic electron precipitation, *J. Geophys. Res.*, *102*, 7421-7430, 1997.

Banks, P. M., and G. Kockarts, *Aeronomy*, Part A, Academic, New York, 1973.

Basu, B., J. R. Jasperse, R. M. Robinson, R. R. Vondrak, and D. S. Evans, Linear transport theory of auroral proton precipitation: A comparison with observations, *J. Geophys. Res.*, *92*, 5920-5932, 1987.

Basu, B., J. R. Jasperse, D. J. Strickland, and R. E. Daniell, Transport-theoretic model for the electron-proton-hydrogen atom aurora, 1. Theory, *J. Geophys. Res.*, *98*, 21517-21532, 1993.

Berger, M. J., S. M. Seltzer, and K. Maeda, Energy deposition by auroral electrons in the atmosphere, *J. Atmos. Terr. Phys.*, *32*, 1015-1045, 1970.

Bilitza, D. (Ed.), *International Reference Ionosphere 1990*, NSSDC 90-22, Natl. Space Sci. Data Cent., Greenbelt, Md, 1990.

Brekke, A., and J. Moen, Observations of high latitude ionospheric conductances, *J. Atmos. Terr. Phys.*, *55*, 1493-1512, 1993.

Codrescu, M. V., T. J. Fuller-Rowell, R. G. Roble, and D. S. Evans, Medium energy particle precipitation influences on the mesosphere and lower thermosphere, *J. Geophys. Res.*, *102*, 19,977-19,987, 1997.

Creutzberg, F., R. L. Gattinger, F. R. Harris, S. Wozniak, and A. Vallance Jones, Auroral studies with a chain of meridian scanning photometers, 2, Mean distributions of proton and electron aurora as a function of magnetic activity, *J. Geophys. Res.*, *93*, 14,591-14,601, 1988.

Decker, D. T., B. V. Kozelov, B. Basu, J. R. Jasperse, and V. E. Ivanov, Collisional degradation of the proton-H atom fluxes in the atmosphere: A comparison of theoretical techniques, *J. Geophys. Res.*, *101*, 26,947-26,960, 1996.

Doyle, M. A., W. J. Burke, D. A. Hardy, P. F. Bythrow, F. J. Rich, and T. A. Potemra, A simple model of auroral electrodynamics compared with HILAT measurements, *J. Geophys. Res.*, *91*, 6979-6985, 1986.

Fuller-Rowell, T. J., and D. S. Evans, Height-integrated Pedersen and Hall conductivity patterns inferred from the TIROS-NOAA satellite data, *J. Geophys. Res.*, *92*, 7606-7618, 1987.

Galand, M., Transport des protons dans l'ionosphère aurorale, Ph. D. thesis, Univ. Grenoble I, Grenoble, France, 1996.

Galand, M., and A. D. Richmond, Magnetic mirroring in an incident proton beam, *J. Geophys. Res.*, *104*, 4447-4455, 1999.

Galand, M., J. Lilensten, W. Kofman, and R. B. Sidje, Proton transport model in the ionosphere, 1, Multistream ap-

proach of the transport equations, *J. Geophys. Res.*, *102*, 22,261-22,272, 1997.

Galand, M., R. Roble, and D. Lummerzheim, Ionization by energetic protons in Thermosphere-Ionosphere Electrodynamics General Circulation Model, *J. Geophys. Res.*, *104*, 27,973-27,989, 1999.

Gasda, S., and A. D. Richmond, Longitudinal and interhemispheric variations of auroral ionospheric electrodynamics in a realistic geomagnetic field, *J. Geophys. Res.*, *103*, 4011-4021, 1998.

Germany, G. A., D. G. Torr, P. G. Richards, M. R. Torr, and S. John, Determination of ionospheric conductivities from FUV auroral emissions, *J. Geophys. Res.*, *99*, 23,297-23,305, 1994.

Hardy, D. A., M. S. Gussenhoven, and R. Raistrick, Statistical and functional representations of the pattern of auroral energy flux, number flux, and conductivity, *J. Geophys. Res.*, *92*, 12,275-12,294, 1987.

Hardy, D. A., M. S. Gussenhoven, and D. Brautigam, A statistical model of auroral ion precipitation, *J. Geophys. Res.*, *94*, 370-392, 1989.

Hardy, D. A., W. McNeil, M. S. Gussenhoven, and D. Brautigam, A statistical model of auroral ion precipitation 2. Functional representation of the average patterns, *J. Geophys. Res.*, *96*, 5539-5547, 1991.

Hedin, A. E., Extension of the MSIS thermosphere model into the middle and lower atmosphere, *J. Geophys. Res.*, *96*, 1159-1172, 1991.

Jasperse, J. R., and B. Basu, Transport theoretic solutions for auroral proton and H atom fluxes and related quantities, *J. Geophys. Res.*, *87*, 811-822, 1982.

Jones, A. V., *Aurora*, D. Reidel, Norwell, Mass., 1974.

Kozelov, B. V., and V. E. Ivanov, Monte Carlo calculation of proton-hydrogen atom transport in N_2, *Planet. Space Sci.*, *40*, 1503-1511, 1992.

Langel, R. A., International Geomagnetic Reference Field: The sixth generation, *J. Geomagn. Geoelectr.*, *44*, 679-707, 1992.

Lilensten, J., and M. Galand, Proton-electron precipitation effects on the electron production and density above EISCAT (Tromsø) and ESR, *Ann. Geophys.*, *16*, 1299-1307, 1998.

Newell, P. T., W. J. Burke, C.-I. Meng, E. R. Sanchez, and M. E. Greenspan, Identification and observations of the plasma mantle at low altitude, *J. Geophys. Res.*, *96*, 35-45, 1991.

Oran, E. S., V. B. Wickwar, W. Kofman, and A. Newman, Auroral plasma lines: A first comparison of theory and experiment, *J. Geophys. Res.*, *86*, 199-205, 1981.

Pesnell, W. D., K. Omidvar, and W. R. Hoegy, Momentum transfer collision frequency of O^+-O, *Geophys. Res. Lett.*, *20*, 1343-1346, 1993.

Rees, M. H., Auroral ionization and excitation by incident energetic electrons, *Planet. Space Sci.*, *11*, 1209-1218, 1963.

Rees, M. H., *Physics and Chemistry of the Upper Atmosphere*, *Cambridge Atmos. Space Sci. Ser.*, Cambridge Univ. Press, New York, 1989.

Rees, M. H., D. Lummerzheim, and R. G. Roble, Modeling of the atmosphere-magnetosphere-ionosphere system MAMI, *Space Sci. Rev.*, *71*, 691-703, 1995.

Reiff, P. H., Models of auroral-zone conductances, in *Magnetospheric Currents*, Geophys. Monogr. Ser., vol. 28, edited by T. A. Potemra, pp. 180-191, AGU, Washington, D.C., 1984.

Rich, F. J., M. S. Gussenhoven, and M. E. Greenspan, Using simultaneous particle and field observations on a low altitude satellite to estimate Joule heat energy flow into the high latitude ionosphere, *Ann. Geophys.*, *6*, 527-534, 1987.

Rich, F. J., M. S. Gussenhoven, D. A. Hardy, and E. Holeman, Average height-integrated Joule heating rates and magnetic deflection vectors due to field-aligned currents during sunspot minimum, *J. Atmos. Terr. Phys.*, *53*, 293-308, 1991.

Richmond, A. D., Ionospheric electrodynamics, in *Handbook of Atmospheric Electrodynamics*, vol. 2, edited by H. Volland, pp. 249-290, CRC Press, Boca Raton, Fla., 1995.

Richmond, A. D., and Y. Kamide, Mapping electrodynamics features of the high-latitude ionosphere from localized observations: technique, *J. Geophys. Res.*, *93*, 5741-5759, 1988.

Richmond, A. D., E. C. Ridley, and R. G. Roble, A thermosphere/ionosphere general circulation model with coupled electrodynamics, *Geophys. Res. Lett.*, *19*, 601-604, 1992.

Robinson, R. M., and R. R. Vondrak, Characteristics and sources of ionization in the continuous aurora, *Radio Sci.*, *20*, 447-455, 1985.

Robinson, R. M., R. R. Vondrak, K. Miller, T. Dabbs, and D. Hardy, On calculating ionospheric conductances from the flux and energy of precipitating electrons, *J. Geophys. Res.*, *92*, 2565-2569, 1987.

Senior, C., Solar and particle contributions to auroral height-integrated conductivities from EISCAT data: A statistical study, *Ann. Geophys.*, *9*, 449-460, 1991.

Senior C., J. R. Sharber, O. De La Beaujardière, R. A. Heelis, D. S. Evans, J. D. Winningham, M. Sugiura, and W. R. Hoegy, *E* and *F* region study of the evening sector auroral oval: A Chatanika/Dynamics Explorer 2/NOAA 6 comparison, *J. Geophys. Res.*, *92*, 2477-2494, 1987.

Søraas, F., H. R. Lindalen, K. Måseide, A. Egeland, T. A. Sten, and D. S. Evans, Proton precipitation and the H_β emission in a postbreakup auroral glow, *J. Geophys. Res.*, *79*, 1851-1859, 1974.

Strickland, D. J., R. E. Daniell Jr., J. R. Jasperse, and B. Basu, Transport-theoretic model for the electron-proton-hydrogen atom aurora, 2, Model results, *J. Geophys. Res.*, *98*, 21,533-21,548, 1993.

Urban, A., Measurements of low energy auroral ions, *Planet. Space Sci.*, *29*, 1353-1365, 1981.

Vickrey, J. F., R. R. Vondrak, and S. J. Matthews, The diurnal and latitudinal variation of auroral zone ionospheric conductivity, *J. Geophys. Res.*, *86*, 65-75, 1981.

Vickrey, J. F., R. R. Vondrak, and S. J. Matthews, Energy deposition by precipitating particles and Joule dissipation in the auroral ionosphere, *J. Geophys. Res.*, *87*, 5184-5196, 1982.

Wallis, D. D., and E. E. Budzinski, Empirical models of height integrated conductivities, *J. Geophys. Res.*, *86*, 125-137, 1981.

Watermann, J., O. De La Beaujardière, and F. J. Rich, Comparison of ionospheric electrical conductances inferred from coincident radar and spacecraft measurements and photoionization models, *J. Atmos. Terr. Phys.*, *55*, 1513-1520, 1993.

Wickwar, V. B., M. J. Baron, and R. D. Sears, Auroral energy input from energetic electrons and Joule heating at Chatanika, *J. Geophys. Res.*, *80*, 4364-4367, 1975.

M. Galand, Center for Space Physics, Boston University, 725 Commonwealth Avenue, Boston, MA 02215. (mgaland@bu.edu)

A.D. Richmond, High Altitude Observatory, National Center for Atmospheric Research, 3450 Mitchell Lane, Boulder, CO 80301.

(Received October 27, 1999; revised January 14, 2000; accepted February 13, 2000.)